D. F. Socie, P. Kurath,* and J. Koch**

A Multiaxial Fatigue Damage Parameter

REFERENCE Socie, D. F., Kurath, P., and Koch, J., **A multiaxial fatigue damage parameter**, *Biaxial and Multiaxial Fatigue*, EGF 3 (Edited by M. W. Brown and K. J. Miller), 1989, Mechanical Engineering Publications, London, pp. 535–550.

ABSTRACT An extension of a shear strain based multiaxial fatigue damage parameter employing three nominal stress–strain terms is presented. The maximum shear strain amplitude, the primary damage parameter, is modified by the strain amplitude and mean stress normal to the maximum shear strain amplitude plane. Fifteen tension–torsion loading paths were chosen to validate the format of the proposed damage parameter. Fatigue cracks were observed to form and grow on the plane of maximum shear strain amplitude when 55 Inconel 718 tubular specimens were tested in strain control. Fractographic examination and crack growth measurements are presented to support the proposed damage model which correlated the data to within a factor of two.

Introduction

At the First International Symposium on Multiaxial Fatigue the tension–torsion fatigue behaviour of Inconel 718 was reported for fully reversed and zero to maximum tension, torsion, and combined loadings (**1**). This paper presents data for a wider variety of loading histories and strain amplitudes. Data are correlated in terms of a critical shear plane theory. Several critical plane theories have been proposed; Sultan (**2**), Findley (**3**), Troost (**4**), Grubisic (**5**), Brown and Miller (**6**), and Lohr and Ellison (**7**). All of them are based on a critical plane for crack nucleation and growth but differ in the format of the damaging parameters. Since the deformation observed for these tests displays plastic strain, a strain based theory seems appropriate. Brown and Miller proposed that the maximum shear strain governed plastic deformation and, hence, crack initiation. Once the crack formed, they reasoned that it would be assisted in propagation by the normal strain on the maximum shear strain amplitude plane. In an extension of the original theory (**8**), Kandil *et al.* presented a general equation for the equivalent shear strain amplitude for a given fatigue life in of the form

$$\hat{\gamma} + S\hat{\varepsilon}_n = \text{constant} \tag{1}$$

The constant, S, is determined experimentally. A mean stress term $T\hat{\sigma}_{no}/E$ was added to incorporate mean stress effects in the analysis (**1**). The parameter T is also an experimentally obtained constant. These damage parameters can then

* Department of Mechanical and Industrial Engineering, University of Illinois at Urbana-Champaign, West Green Street, Urbana, IL 61801, USA.

Table 1 Base line material properties, IN–718

Monotonic tensile properties		
E	Elastic modulus	208 500 MPa
$\sigma_{y0.2\%}$	0.2 per cent offset yield strength	1160 MPa
σ_u	Ultimate strength	1420 MPa
σ_f	True fracture strength	1850 MPa
ε_f	True fracture strain	0.330
% RA	% reduction in area	28
K	Strength coefficient	1910 MPa
n	Strain hardening exponent	0.08
R_c	Rockwell hardness	40
Torsional cyclic properties ($R_\gamma = -1$)		
G	Torsional modulus	77 800 MPa
τ_f'	Fatigue strength coefficient	2146 MPa
b_o	Fatigue strength exponent	−0.148
γ_f'	Fatigue ductility coefficient	18.0
c_o	Fatigue ductility exponent	−0.922
A'	Cyclic strength coefficient	860 MPa
n_o'	Cyclic strain hardening exponent	0.079

be combined with the torsional strain–life curve with the following result

$$\hat{\gamma} + S\hat{\varepsilon}_n + \frac{T\hat{\sigma}_{no}}{E} = \gamma_f'(2N_{1.0})^{c_o} + \frac{\tau_f'}{G}(2N_{1.0})^{b_o} \tag{2}$$

The shear fatigue properties of the material are analogous to the uniaxial fatigue parameters given in ASTM E606 and are determined from fully reversed torsion tests. Both $\hat{\varepsilon}_n$ and $\hat{\sigma}_{no}$ are zero during a torsion test. The constants S and T can be evaluated by comparing fully reversed torsional data to uniaxial tests at strain ratios of $R_\varepsilon = -1$ ($\hat{\varepsilon}_n \neq 0$, $\hat{\sigma}_{no} = 0$) and $R_\varepsilon = 0$ ($\hat{\varepsilon}_n \neq 0$, $\hat{\sigma}_{no} \neq 0$). Strain–life constants for equation (2) are given in Table 1.

The conceptual basis for the model is schematically shown in Fig. 1. During shear loading, the irregularly shaped crack surface results in frictional forces which reduce crack tip stresses, thus retarding crack growth and increasing the fatigue life. Normal stresses and strains will separate the crack surfaces and reduce frictional forces which will increase the crack growth rate. Metallurgical sectioning **(9)**–**(11)** was performed on this material to show that the cracks nucleate and initially grow on the planes of maximum shear strain amplitude. Fractographic evidence for the influence of normal stress and strain is presented in Fig. 2. The torsion test fractograph exhibits extensive rubbing and is featureless in contrast to the tensile test fractograph, where individual slip bands are observed on the fracture surface.

This paper presents two new aspects of our work. Namely, the validation of the model for lower strain levels where the plastic strains are negligible, and a wider variety of multiaxial loading histories. Details on the material, specimen,

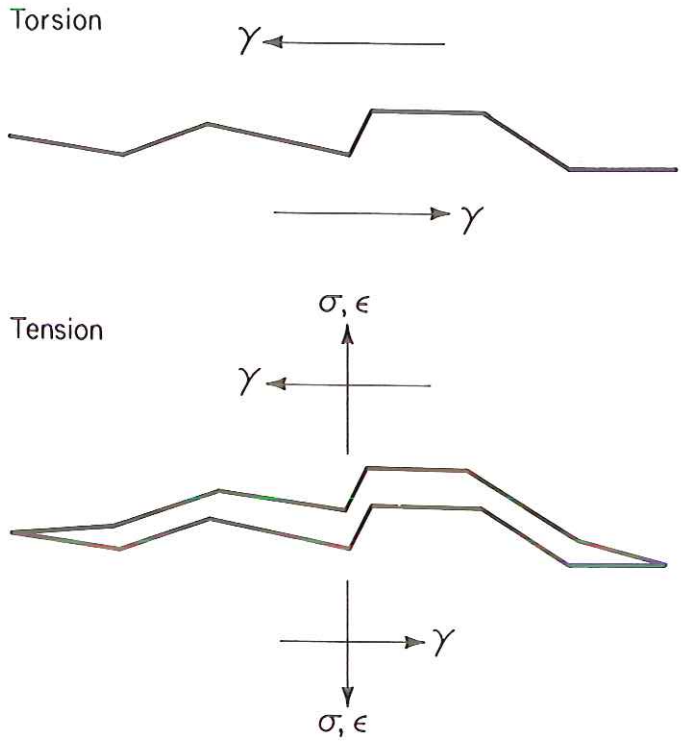

Fig 1 Schematic illustration of the effect of normal stress and strain on shear cracks

extensometry, and testing procedure are presented in a previous publication (1). Results of all tension–torsion tests conducted using Inconel 718 are given in Table 2.

Notation

A'	Cyclic torsional strength coefficient
b_o	Torsional fatigue strength exponent
c_o	Torsional fatigue ductility exponent
E, G	Axial, shear elastic modulus
S, T	Biaxial material properties
$2N_{1.0}$	Number of reversals to a 1.0 mm crack length
$N_{1.0}, N_f$	Number of cycles to 1.0 mm crack length, failure
n'_o	Torsional, cyclic strain hardening exponent
$\hat{\gamma}$	Maximum shear strain amplitude
γ'_f	Torsional fatigue shear ductility coefficient

Table 2 Biaxial fatigue data, IN–718

		Midsection values									
		Control parameters				*Steady-state stresses*					
Path code	*Spec ID*	$\Delta\varepsilon/2$	ε_o	$\Delta\gamma/2$	γ_o	$\Delta\sigma/2$ (*MPa*)	σ_o (*MPa*)	$\Delta\tau/2$ (*MPa*)	τ_o (*MPa*)	$N_{1.0}$ (*cycles*)	N_f (*cycles*)
A	B-33	0.0100	0	0	0	1090	−30	0	0	1000	1230
	B-14	0.0100	0	0	0	1100	−23	0	0	1050	1330
	B-6	0.0050	0	0	0	924	−19	0	0	13 500	14 200
	B-12	0.0050	0	0	0	931	−30	0	0	11 000	13 400
B	B-7	0	0	0.0176	0	0	0	605	5	890	1690
	B-13	0	0	0.0176	0	0	0	596	0	800	1670
	B-3	0	0	0.0087	0	0	0	538	1	7200	10 600
	B-8	0	0	0.0087	0	0	0	535	−12	7000	12 900
	A-35	0	0	0.0054	0	0	0	416	10	34 000	41 400
	A-30	0	0	0.0054	0	0	0	414	−20	35 700	45 200
	A-16	0	0	0.0043	0	0	0	324	−18	105 000	131 000
	A-02	0	0	0.0038	0	0	0	285	−40	114 000	223 000
C	B-35	0.0071	0	0.0123	0	752	−29	435	34	1000	1370
	B-11	0.0071	0	0.0123	0	758	−26	427	−3	1200	1580
	B-26	0.0035	0	0.0061	0	633	−87	376	34	8000	12 900
	B-4	0.0035	0	0.0661	0	633	−26	400	−2	7000	12 100
	A-14	0.0015	0	0.0027	0	334	8	199	−9	160 000	178 000
	A-98	0.0015	0	0.0027	0	318	−10	202	−2	290 000	323 000
D	B-5	0.0100	0.0100	0	0	1083	19	0	0	800	936
	B-9	0.0100	0.0100	0	0	1089	22	0	0	800	959
	B-36	0.0050	0.0050	0	0	965	215	0	0	7000	7030
	B-15	0.0050	0.0050	0	0	944	215	0	0	6000	8000
E	B-99	0	0	0.0173	0.0173	0	0	580	14	1000	1690
	B-16	0	0	0.0173	0.0173	0	0	568	14	800	1740
	B-32	0	0	0.0087	0.0087	0	0	507	76	4500	9530

	B-25	0	0	0.0087	0.0087	0	0	502	81	6500	10 800
	A-18	0	0	0.0043	0.0043	0	0	315	305	48 000	82 100
	A-24	0	0	0.0037	0.0037	0	0	285	235	110 000	143 000
F	B-98	0.0071	0.0071	0.0123	0.0123	751	119	419	−71	1050	1330
	B-10	0.0071	0.0071	0.0123	0.0123	779	8	432	7	1000	1500
	B-34	0.0035	0.0035	0.0063	0.0063	646	170	396	52	4800	5960
	B-17	0.0035	0.0035	0.0063	0.0063	632	68	383	102	7500	9500
	A-07	0.0015	0.0015	0.0026	0.0026	311	327	190	198	53 000	67 400
G	B-31	0.0035	−0.0035	0.0063	−0.0063	598	−190	381	−43	6000	14 100
	B-23	0.0035	−0.0035	0.0063	−0.0063	594	−213	375	−29	7000	16 000
H	B-18	0.0035	0	0.0063	0.0063	631	−216	386	139	5000	9140
	B-19	0.0035	0	0.0063	0.0063	632	−189	381	138	5000	7420
I	B-21	0.0035	0	0.0063	0.0063	637	84	389	126	4000	7680
	B-30	0.0035	0	0.0063	0.0063	631	97	398	120	4000	8000
J	B-24	0.0035	0.0035	0.0063	0	638	218	394	−71	3000	5150
	B-29	0.0035	0.035	0.0063	0	637	279	413	−85	3000	3490
K	A-36	0	0.0010	0.0086	0	0	75	504	−42	6500	8370
	A-34	0	0.0010	0.0086	0	0	63	505	−4	7470	10 900
	A-11	0	0.0015	0.0038	0	0	335	287	−10	52 000	58 700
L	A-31	0	−0.0010	0.0086	0	0	−172	507	0	3890	8000
	A-33	0	−0.0010	0.0086	0	0	−161	513	0	9090	13 100
	A-19	0	−0.0015	0.0038	0	0	−329	274	−33	462 000	590 000
M	A-32	0.0035	0	0.0062	0	520	−10	495	31	5550	6700
	A-29	0.0035	0	0.0062	0	510	−28	496	25	6080	6990
N	B-97	0.0071	0	0.0123	0	999	−29	552	1	430	565
	B-20	0.0071	0	0.0123	0	999	−32	567	−8	450	560
	B-28	0.0035	0	0.0062	0	758	−19	463	−10	4370	5810
	B-27	0.0035	0	0.0062	0	758	−34	463	1	3350	5150
O	A-28	0.0035	0.0035	0.0062	0	724	283	450	−7	3550	4450
	A-27	0.0035	0.0035	0.0062	0	724	308	450	−4	3330	3850

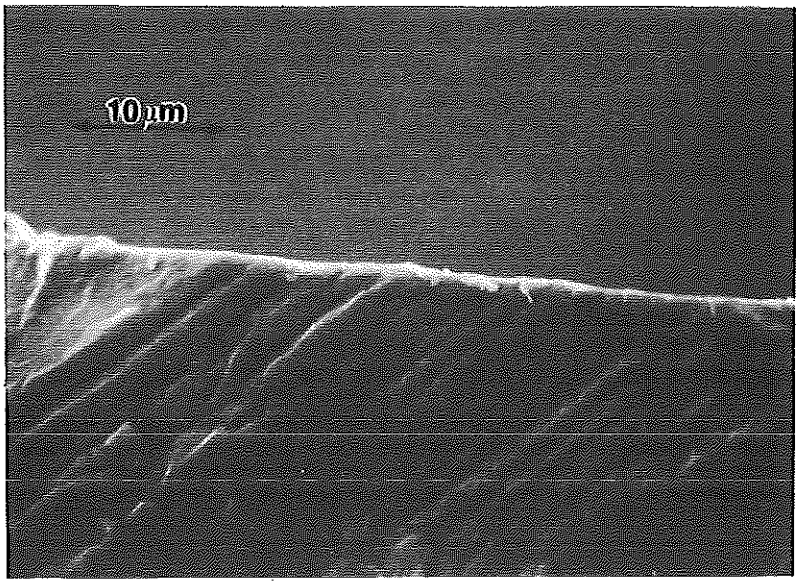

(a)

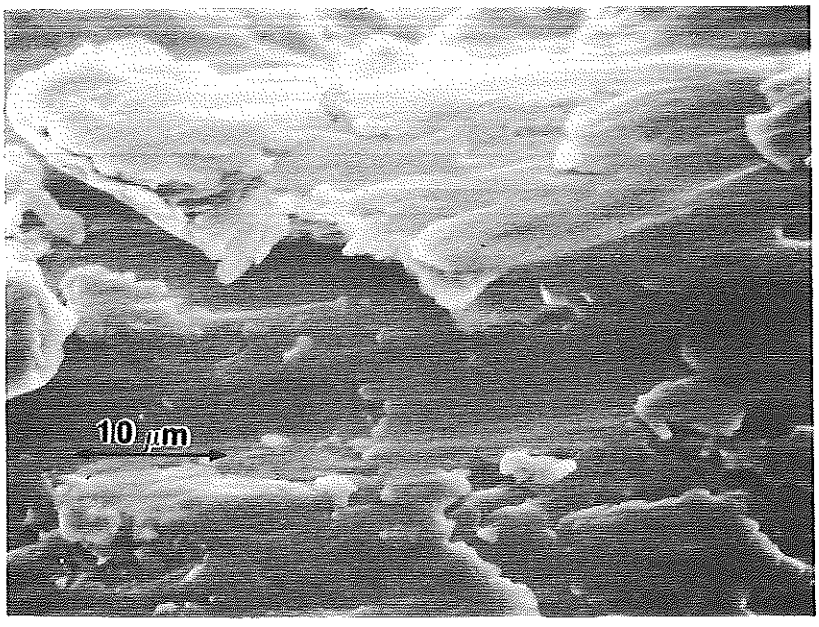

(b)

Fig 2 Comparison of maximum shear strain amplitude plane fracture surfaces for (a) tension, and (b) torsion

$\hat{\varepsilon}_n$	Strain amplitude normal to the plane of maximum shear strain amplitude
λ	Strain ratio; shear strain amplitude/axial strain amplitude
$\hat{\sigma}_{no}$	Mean stress normal to the plane of maximum shear strain, amplitude
τ'_f	Torsional fatigue shear strength coefficient
Φ	Phase difference between axial and torsional strain maximums

Results and discussion

Biaxial strain path selection

Selection of the fifteen strain paths shown in Fig. 3 was a continuous process based on results from prior testing. As the investigation progressed, physical characteristics of crack growth were evaluated in the light of the known stress/strain states in order to identify additional critical strain paths. Some critical tests were proposed to isolate one variable at a time from equation (2).

Cracking characteristics and other biaxial material baseline data were obtained from fully-reversed proportional paths A–C. Torsion tests (path B) provided data where the maximum shear strain amplitude planes had zero normal strains and stresses. This test allowed evaluation of the biaxial damage criteria (equation (2)) without consideration of non-shear terms. Crack formation and growth were observed to occur on $\hat{\gamma}$ planes. Fully reversed tension tests (path A) were employed to observe correlation between thin wall tubes and uniaxial smooth specimens. Again, nearly all fatigue crack growth (which was

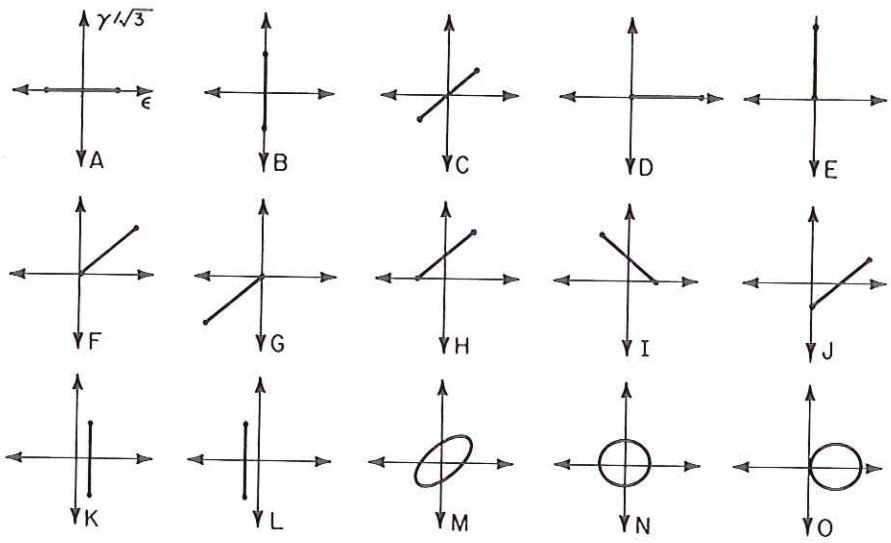

Fig 3 Tension–torsion loading histories

the majority of the fatigue life) was observed on $\hat{\gamma}$ planes. Strains normal to the $\hat{\gamma}$ plane were present for these tests, and the $\hat{\varepsilon}_n$ term allowed correlation with previous torsional data and calculation of the constant S. Proportional combined tension–torsion tests with $\lambda = \sqrt{3}$ (path C) followed as the simplest combination of paths A and B. These tests further established the crack growth direction as occurring on planes of maximum shear strain amplitude.

Further investigation of non-shear effects was accomplished with proportional mean strain paths D and F where the mean stress term, $\hat{\sigma}_{no}$, was isolated for study. Directions and magnitudes of $\hat{\gamma}$ and $\hat{\varepsilon}_n$ were not altered by the mean strains, allowing comparison with paths A and C and calculation of the constant T. Effects of different mean strains and stresses during combined tension–torsion loading were evaluated through simple modifications of path C. Paths G–J were chosen such that the axial and torsional strain amplitudes, and $\lambda = \sqrt{3}$ were identical. These tests strengthened the confidence in the form of non-shear terms. Crack growth for these mean stress and strain paths was in the $\hat{\gamma}$ direction (**12**).

Paths K and L were employed to identify whether the form of the normal strain term, $\hat{\varepsilon}_n$, should be an amplitude or maximum. If $\hat{\varepsilon}_n$ was an amplitude term, fatigue damage predicted from static axial strains would be zero. Mean stresses due to static axial strains resulted on the 0 degree plane (normal to the specimen axis), but were zero on the 90 degree plane. Out-of-phase paths M–O were employed to evaluate phase dependency of the proposed parameters. Rotating $\hat{\gamma}$ planes with respect to specimen orientation would result in non-zero values of shear strain for all planes. However, one $\hat{\gamma}$ plane was always preferred for long crack growth.

Cracking characteristics

Two characteristics of fatigue cracks, their direction and growth rate, were evaluated in this investigation. Fatigue crack initiation and growth were observed to occur on or near planes of maximum shear strain amplitude in all tests. Only tension tests displayed stage II behaviour late in the fatigue life. This deviation in crack direction accounted for approximately 5 per cent of the fatigue life to form a surface crack 1.0 mm long and is considered to be insignificant for this material at the strain ranges investigated.

Crack growth for fully reversed proportional paths A–C occurred on both $\hat{\gamma}$ planes (**1**). Mean strain, proportional paths D–F demonstrated fatigue crack growth behaviour similar to paths A–C, differing only by preferred crack growth on the $\hat{\gamma}$ plane which had the larger non-shear terms. Fatigue crack growth for non-proportional linear strain paths G–J followed suit closely with cracks growing near $\hat{\gamma}$ planes. When both $\hat{\gamma}$ planes experienced tensile normal mean stresses (path J), the orientation with the larger mean stress experienced accelerated crack growth, in comparison to the cracks growing on the other $\hat{\gamma}$ plane. Conversely, when both planes experienced compressive normal mean stresses, (path G) crack growth was retarded and a large number of cracks

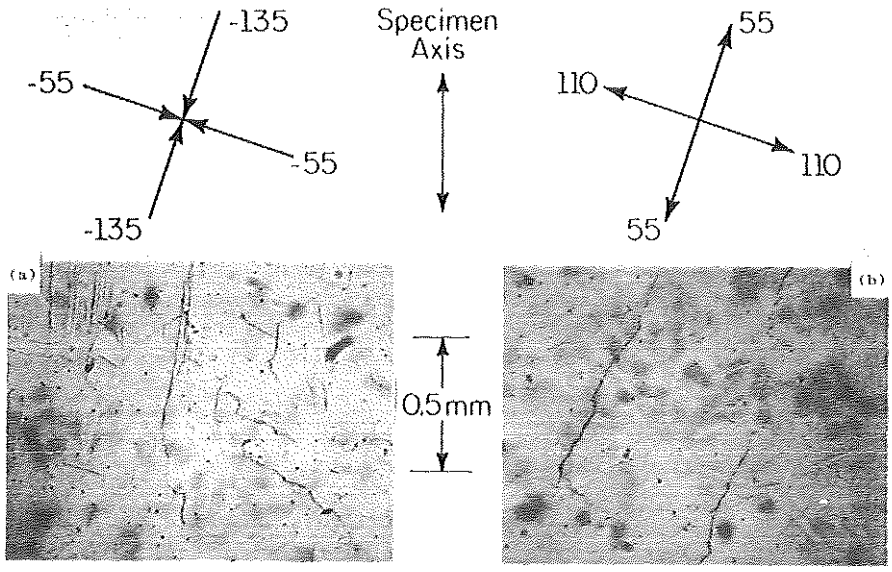

Fig 4 The effect of mean stress on crack formation using (a) path F, and (b) path G

formed. Crack growth on the plane with the least compressive mean stress was retarded to a lesser degree with final failure occurring on that plane. Crack density for this case was much higher on both $\hat{\gamma}$ planes than for those tests with tensile mean stresses across the $\hat{\gamma}$ planes. This behaviour is qualitatively shown in Fig. 4. The magnitude and direction of the mean stresses are shown at the top of each photo.

Fatigue cracks in torsion have been observed to form on both maximum shear planes and then propagate to failure on the plane parallel to the specimen axis (90 degree plane). The preference to the 90 degree plane may be due to a slight tensile mean hoop stress that is ignored in simple thin tube analysis. Torsion tests with a static axial strain, paths K and L, demonstrated similar crack formation behaviour. Fully reversed torsion (path B) and torsion with a static compressive mean stress (path L) displayed identical cracking direction. Late in the fatigue life of path K, which had a static tensile axial strain, the crack that propagated to failure was on the $\hat{\gamma}$ plane normal to the specimen axis (0 degree plane). This behaviour was attributed to the tensile normal mean stress across the 0 degree plane, whereas path L had a compressive mean stress across this plane. Figure 5 shows the failure cracks for paths B, K, and L.

Growth of the failure crack for imposed static axial strains (paths B, K, and L) is compared in Fig. 6. No systematic differences were identified. Stress states on the 90 degree plane (i.e., coincident with the specimen axis) were identical for paths B, K, and L (no imposed hoop stress). A tensile mean stress for path L on the 0 degree plane (i.e., normal to the specimen axis) was sufficient to

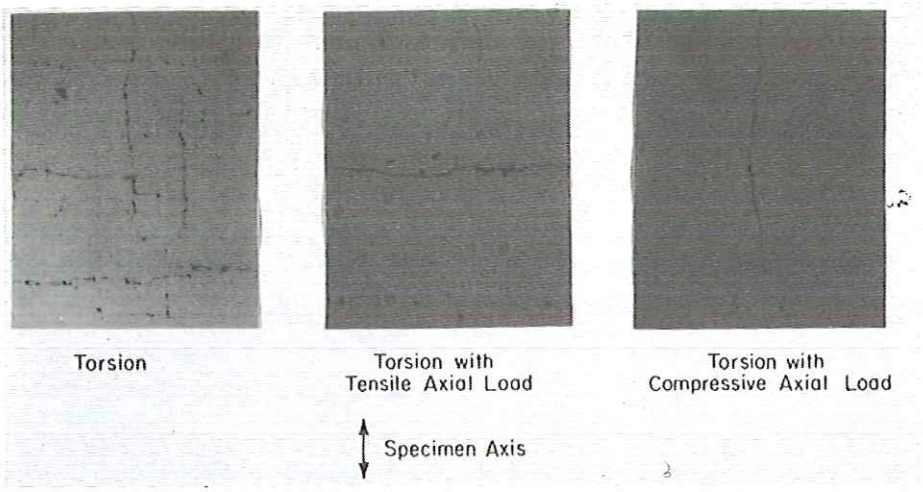

Fig 5 Typical fatigue cracks for strain paths B, K, and L

switch the failure plane, but insufficient to cause noticeable difference in propagation rate. In other words, the $\hat{\gamma}$ plane with the most tensile normal stress was preferred for propagation. Second-order stress terms neglected in the deformation analysis may be responsible for the slight differences in crack growth rates between paths B and L.

For the out-of-phase loadings (paths M, N, and O) the cracks propagated on or near the $\hat{\gamma}$ plane which was experiencing the larger normal stresses and

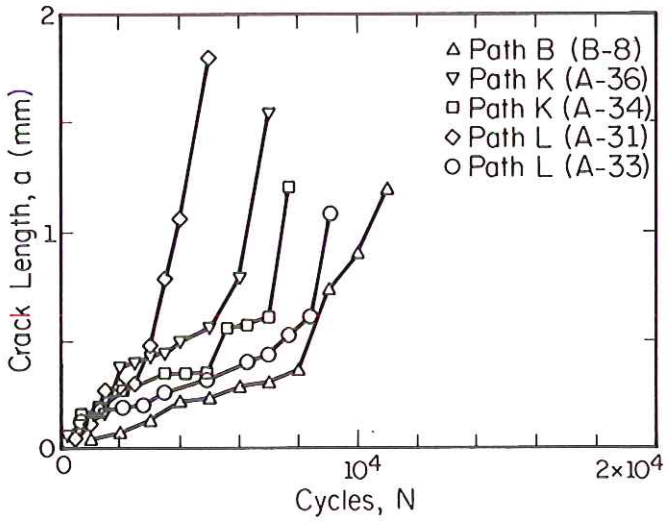

Fig 6 Crack growth data for strain paths B, K, and L

strains. Path M experienced tensile components of normal stress and strain on both $\hat{\gamma}$ planes, but preferred the plane with the greater normal values. For paths N and O, one of the $\hat{\gamma}$ plane is normal to the specimen axis (0 degree plane). This plane experienced the entire applied axial strain and stress, while the 90 degree plane (parallel to the specimen axis) experienced only a Poisson's strain and zero stress according to plane stress assumption. For path N at larger strain amplitudes, many cracks formed early in the fatigue life, with no preferred direction. Upon reaching 0.1 mm, subsequent crack growth was preferred on planes 2–5 degrees away from the 0 degree plane. At lower strain amplitudes, nearly all cracks formed and propagated on the 0 degree plane. Crack density was approximately an order of magnitude less for the smaller amplitude. Fatigue crack growth direction for path 0 was similar to the smaller amplitude case of path N. The greater mean stress on the 0 degree plane accelerated failure growth for path 0, resulting in reduced fatigue life in comparison to a similar strain excursion for path N. Crack density for path 0 was less than that for path N at identical effective strain amplitudes.

Non-proportional out-of-phase paths M, N, and O were compared with combined tension–torsion paths C and J, respectively. Test results with identical axial and torsional strain amplitudes were employed for these comparisons, differing only by the phase angle, Φ. Out-of-phase path M ($\Phi = 45$ degrees) is compared to the path C in Fig. 7. Initial crack growth increments were similar for both strain paths. At a crack length of approximately 0.2 mm, accelerated crack growth occurred for the out-of-phase tests. Mean stresses and strain amplitudes normal to the crack plane were deemed to be responsible for this behaviour. Mixed mode shear crack fracture mechanics arguments support the

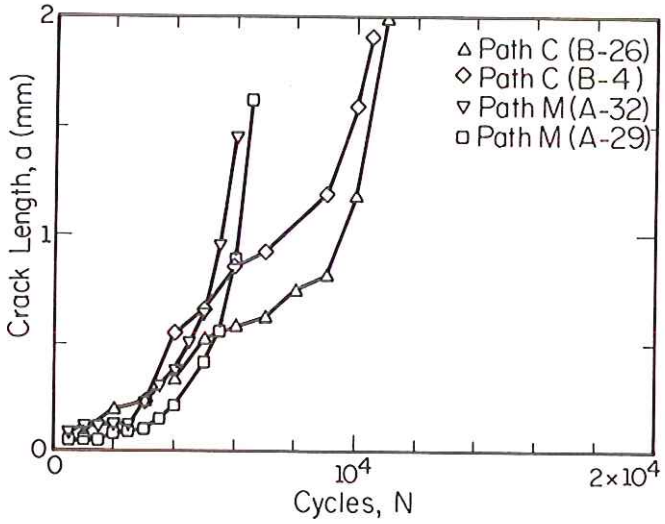

Fig 7 Crack growth data for in-phase (path C) and 45 degree out-of-phase loading (path M) at $\Delta\varepsilon/2 = 0.0035$ and $\Delta\gamma/2 = 0.0062$

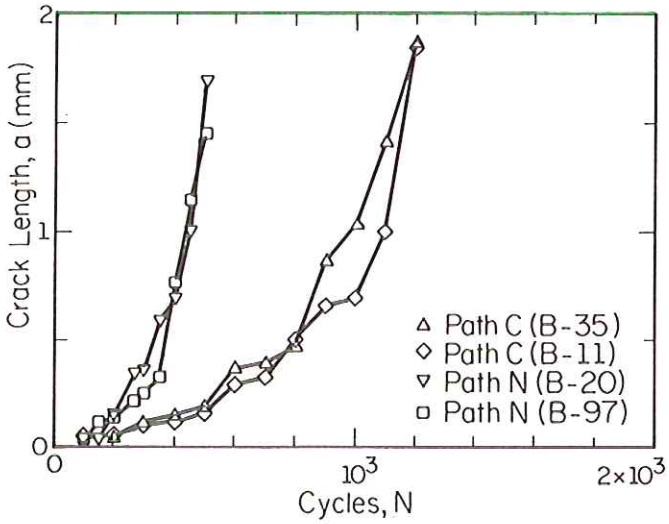

Fig 8 Crack growth data for in-phase (path C) and 90 degree out-of-phase loading (path N) at $\Delta\varepsilon/2 = 0.0071$ and $\Delta\gamma/2 = 0.0123$

notion that the normal stresses and strains became more significant with increasing crack length. Therefore, the differences in crack growth that became more evident at longer crack lengths were expected.

Out-of-phase strain path N (Φ = 90 degrees) was also contrasted with proportional strain path C. Two amplitudes of applied axial and torsional strain are available for comparison (Figs 8 and 9). Trends similar to those observed

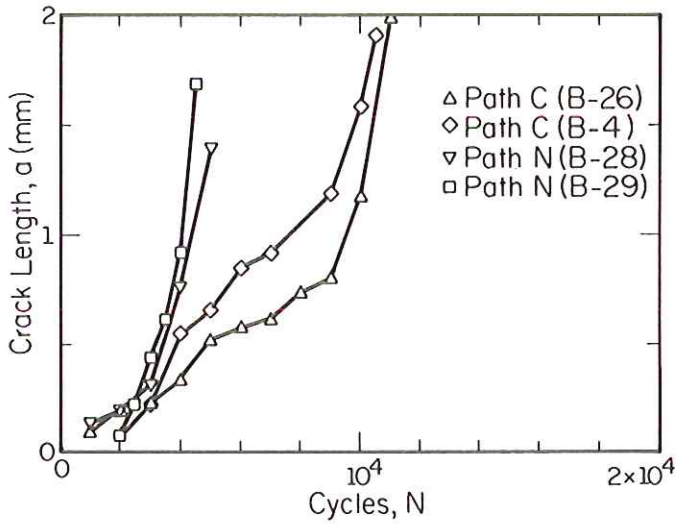

Fig 9 Crack growth data for in-phase (path C) and 90 degree out-of-phase loading (path N) at $\Delta\varepsilon/2 = 0.0035$ and $\Delta\gamma/2 = 0.0062$

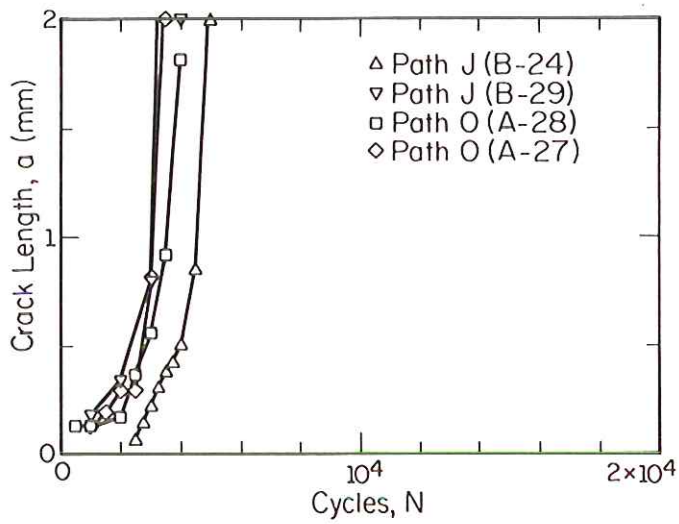

Fig 10 Crack growth data for in-phase (path J) and 90 degree out-of-phase loading (path O) mean stress tests at $\Delta\varepsilon/2 = 0.0035$ and $\Delta\gamma/2 = 0.0062$

between paths M and C were noted at both of these amplitudes. Arguments analogous to those previously forwarded were employed to explain the accelerated crack growth later in the fatigue lives. Due to the nature of the phase angle for path N ($\Phi = 90$ degrees) a greater shear strain amplitude was experienced by the failure crack plane while the crack was being opened by normal stresses and strains than for Path M ($\Phi = 45$ degrees) tests. Damage characteristics were similar, only more severe for Path N.

Out-of-phase path O experienced even greater normal strains and mean stresses on the failure crack plane than did Path N. Comparisons with linear path J are shown in Fig. 10. Crack growth for path O closely matched path J. Path J experienced a damaging combination of shear strain with tensile normal strains and mean stresses, similar to path O. Therefore, the combination of shear excursion with a tensile strain and mean stress normal to the crack plane caused increased damage, not the out-of-phase loading.

Life prediction

A crack length of 1.0 mm was employed as a reference to compare fatigue lives from all the different strain paths. The shear damage model (equation (2)) was employed to evaluate the experimental results. Fifty-five test results are shown on the plot in Fig. 11. Total shear strain amplitude from fully reversed torsional tests (Path B) were employed to generate the baseline damage curve (solid line in Fig. 11). Baseline data were taken from strain path B because stresses and strains normal to the $\hat{\gamma}$ planes are zero. Elastic and plastic strains were fit by a least squares method to obtain material constants (Table 1) and then summed in a similar fashion to uniaxial $\varepsilon - N_f$ diagrams. Constant amplitude uniaxial

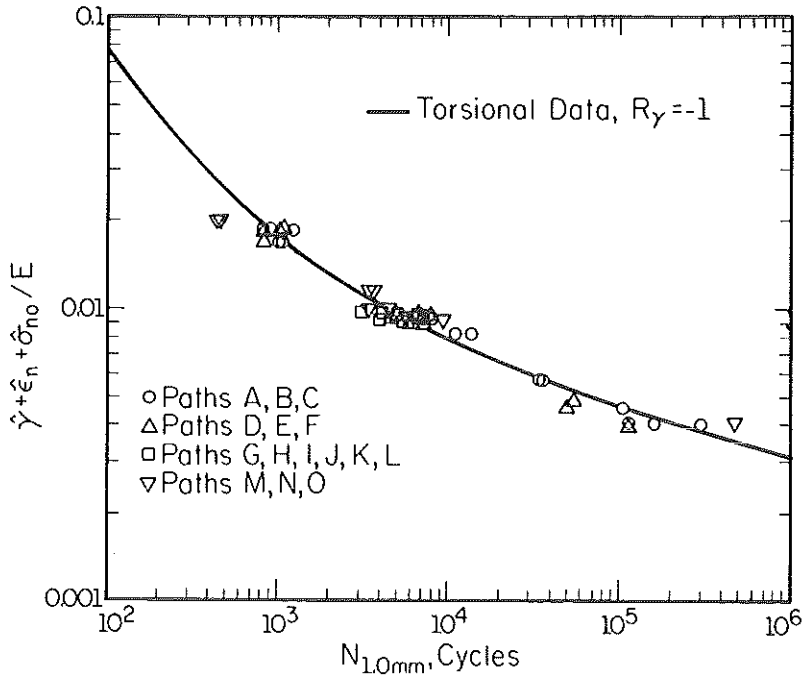

Fig 11 Correlation of test data employing a maximum shear strain amplitude based damage parameter which also incorporates strain amplitude and mean stress normal to the maximum shear amplitude plane

testing showed that the constants S and T may be taken as unity in equation (1). The solid line represents the fully reversed torsional baseline data. Most tests demonstrated good correlation with this damage model. Exceptions included a systematic inability to account for large amounts of plasticity in out-of-phase tests (Path N). This is probably due to the out-of-phase hardening which increases the cyclic normal stress range while the cyclic normal strain range and normal stress remain constant.

It is important to note that degree of correlation presented here is only possible because the model matches the physical damage process, which is crack nucleation and growth on planes of maximum shear strain amplitude. This model is not appropriate for materials which may nucleate in shear, but spend the majority of life in mode I tensile crack growth. Bannantine and Socie (**13**) have shown that 304 stainless steel is such a material and that the shear based parameter provides poor correlation of the data. Instead, they modified the Smith–Watson–Topper parameter (**14**) to describe the tensile cracking in 304 stainless steel.

Conclusions

(1) The majority of the fatigue life of Inconel 718 tubular specimens is spent in growing cracks from 0.01 to 1.0 mm on planes of maximum shear strain amplitude for the range of fatigue lives under consideration (10^3–10^6 cycles).
(2) The cyclic tensile strain perpendicular to the shear crack enhances its growth and reduces the fatigue life.
(3) Mean tensile stress perpendicular to the shear crack also enhances its growth and reduces the fatigue life.
(4) The physical damage mechanism, shear crack formation and growth is reflected in the choice of nominal stress and strain terms employed in the proposed damage model. Comparable correlation of multiaxial data using the proposed damage parameter is not anticipated for materials which do not display similar physical damage phenomena.

Acknowledgements

All the experiments were conducted in the Materials Engineering Research Laboratory at the University of Illinois, Urbana-Champaign. Allison Gas Turbine Co., Indianapolis, IN, provided the material and funding for this research. The Mechanical Engineering Department Publications Office assisted in the preparation of this manuscript.

References

(1) SOCIE, D. F., WAILL, L. A., and DITTMER, D. F. (1985) Biaxial fatigue of Inconel 718 including mean stress effects, *Multiaxial Fatigue, ASTM STP 853*, ASTM, Philadelphia, PA, pp, 463–481.
(2) STULEN, F. B. and CUMMINGS, H. N. (1954) *Proceedings, ATMS*, **54**, 822–829.
(3) FINDLEY, W. N. (1959) *J. Engng Ind.*, **81**, 301–306.
(4) TROOST, A. and EL-MAGD, E. (1976) Beurteilung det Schwingfestigkeit bei mehrachsiger Beanspruchung auf der Grundlage kritischer Schubspannangen, *Metall.*, 37–41.
(5) GRUBISIC, V. and SIMBÜRGER, A. (1976) Fatigue under combined out of phase multiaxial stresses fatigue testing and design, SEE Int. Conference, The City University, London, Vol. 2, pp. 27.1–27.28.
(6) BROWN, M. W. and MILLER, K. J. (1973) A theory for fatigue failure under multiaxial stress–strain conditions, *Proc. Instn mech. Engrs*, **187**, 745–755.
(7) LOHR, R. D. and ELLISON, E. G. (1980) *Fatigue of Engng Mater. Structures*, **3**, 1–17.
(8) KANDIL, F. A., BROWN, M. W., and MILLER, K. J. (1982) Biaxial low-cycle fatigue fracture of 316 stainless steel at elevated temperatures, Vol. 280, The Metals Society, London, pp. 203–210.
(9) BEER, T. A. (1984) *Crack shapes during biaxial fatigue*, MSc thesis, Department of Mechanical Engineering, University of Illinois at Urbana-Champaign, Urbana, IL, USA.
(10) SOCIE, D. F., HUA, C., BEER, T. A., and WAILL, L. E. (1984) Observations of small cracks in biaxial fatigue, *Second International Conference on Fatigue and Fatigue Tresholds*, pp. 835–845.
(11) WORTHERM, D. W., ALTSTETTER, C. J., ROBERTSON, I. M., and SOCIE, D. F. (1985) Cyclic deformation and damage structure in Inconel 718, presented at Second International Conference on Biaxial/Multiaxial Fatigue.

(12) SOCIE, D. F. and SHIELD, T. W. (1984) Mean stress effects in biaxial fatigue of Inconel 718, *J. Engng Mater. Technol.*, **106**, 227–232.
(13) BANNANTINE, J. A. and SOCIE, D. F. (1988) Observations of cracking behavior in tension and torsion low cycle fatigue, *Low Cycle Fatigue, ASTM STP 924*, ASTM, Philadelphia, PA.
(14) SMITH, R. N., WATSON, P., and TOPPER, T. H. (1970) A stress–strain function for fatigue of metals, *J. Materials*, **5**, 767–778.